A natural variant of the sole pyruvate kinase of fission yeast lowers glycolytic flux triggering increased respiration and oxidative-stress resistance but decreased growth

Stephan Kamrad*[1,2], Jan Grossbach*[3], Maria Rodríguez-López[2], StJohn Townsend[1,2], Michael Mülleder[1], Valentina Cappelletti[4], Gorjan Stojanovski[2], Paola Picotti[4], Andreas Beyer[3,5,#], Markus Ralser[1,6,#], Jürg Bähler[2,#]

[1]The Francis Crick Institute, Molecular Biology of Metabolism Laboratory, London, United Kingdom.
[2]University College London, Department of Genetics, Evolution & Environment, Institute of Healthy Ageing, and UCL Genetics Institute, London WC1E 6BT, United Kingdom.
[3]CECAD, University of Cologne, Cologne, Germany.
[4]Institute of Molecular Systems Biology, Department of Biology, ETH Zurich, Zurich, Switzerland.
[5]Center for Molecular Medicine Cologne, Cologne, Germany.
[6]Charité University Medicine, Berlin, Germany.

*These authors contributed equally
#Corresponding authors

Abstract

Cells balance glycolysis with respiration to support their energetic and biosynthetic needs in different environmental or physiological contexts. With abundant glucose, many cells prefer to grow by aerobic glycolysis, or fermentation in yeast. Using 161 natural isolates of fission yeast, we investigated the genetic basis and phenotypic effects of the fermentation-respiration balance. The laboratory and a few other strains were more dependent on respiration. This trait was associated with a missense variant in a highly conserved region of Pyk1. Pyk1 is the single pyruvate kinase in fission yeast, while most organisms possess isoforms with different activity. This variant reduced Pyk1 activity and glycolytic flux. Replacing the 'low-activity' *pyk1* allele in the laboratory strain with the common 'high-activity' allele was sufficient to increase fermentation and decrease respiration. This metabolic reprogramming triggered systems-level adaptations in the transcriptome and proteome, and in cellular phenotypes, including increased growth and chronological lifespan, but decreased resistance to oxidative stress. Thus, low Pyk1 activity provided no growth advantage but stress tolerance, despite increased respiration. The genetic tuning of glycolytic flux by a single-nucleotide change might reflect an adaptive trade-off in a species lacking pyruvate-kinase isoforms.

Introduction

Inter-linked pathways for carbon metabolism generate energy in the form of ATP and fulfil key anabolic roles. Organisms tune their energy metabolism to environmental conditions, including stress or available nutrients, which affects fundamental biological processes such as cell proliferation, stress resistance and ageing[1,2]. Accordingly, aberrant energy metabolism is the cause of multiple human diseases[3–5]. Glycolysis converts glucose to pyruvate, which is further processed in alternate pathways; for example, pyruvate can be converted to ethanol (fermentation) or it can be metabolised in mitochondria via the citric acid cycle and oxidative phosphorylation (respiration). Fermentation and respiration are antagonistically regulated in response to glucose or physiological factors[6,7]. In the presence of ample glucose, many microbes suppress respiration and generate ATP preferentially by glycolysis, even with oxygen available. This metabolic state, called aerobic glycolysis[8], appears paradoxical, because only full glucose oxidation via the citric acid cycle and respiration will maximize the ATP yield generated per glucose. Aerobic glycolysis, found in Crabtree-positive species, may have been selected because it enables higher rates of ATP production[9]. Analogously, human cancer cells typically grow by aerobic glycolysis, known as the Warburg effect[10], thought to increase biosynthetic capacity[11–13]. Proposed explanations for how aerobic glycolysis allows faster proliferation involve efficient resource allocation[14,15] and molecular crowding[16–19], among others[20–22].

Crabtree-positive organisms, including the model yeasts *Saccharomyces cerevisiae* and *Schizosaccharomyces pombe*[23], still require some oxygen and basal respiration for optimal cell proliferation[24]. *S. cerevisiae* cells without mitochondrial genome, and thus without respiratory capacity, feature a 'petite', slow-growth phenotype[25]. *S. pombe* cannot normally grow without a mitochondrial genome[26–28], and blocking oxidative phosphorylation with

antimycin A leads to moderate or strong growth inhibition, respectively, in rich or minimal glucose media[29]. In glucose-limiting conditions, such as stationary phase, the metabolism of yeast cells is reconfigured towards respiration[30,31]. Thus, cells tune the balance between respiration and fermentation to meet their energetic and biosynthetic needs[6] in a more nuanced way than captured by qualitative descriptions of aerobic glycolysis.

Given its impact in health and disease, it is important to understand the genetic and regulatory factors that affect cellular energy metabolism. Here we investigated the genetic basis and physiological implications for the regulatory balance between fermentation and respiration, using our collection of natural S. pombe isolates[32]. A few strains featured a higher reliance on respiration during cellular growth on glucose. This trait was associated with a missense variant in pyruvate kinase (PYK). PYK catalyses the final, ATP yielding step of glycolysis, the conversion of phosphoenolpyruvate to pyruvate. PYK can coordinate the activity of central metabolic pathways[33–35]. Most organisms encode several PYK isoforms that are expressed in specific tissues or developmental stages[36–40]. Work in budding yeast has implied that the switch from a high- to a low-activity PYK isoform causes increased oxygen uptake, triggering a shift from fermentative to oxidative metabolism[33,34]. *S. pombe* possesses only one PYK, Pyk1[41]. Nonetheless, exchanging the Pyk1 variant of the standard laboratory strain triggered increased glycolytic flux, which in turn led to substantial adjustments in the metabolome, transcriptome and proteome. These results show that altered PYK activity is self-sufficient to reprogram metabolism even in the absence of an evolved regulatory signaling system. These findings define a natural metabolic switch, consisting of a single amino-acid change, possibly reflecting an adaptation in a species lacking multiple PYK isoforms. Notably, the standard laboratory strain is among a minority of natural isolates locked in the low-activity state, and is thus metabolically and physiologically unusual. These findings highlight the importance of glycolysis in general, and PYK in particular, as a hub in cross-regulating metabolic pathways and coordinating energy metabolism with cell regulation and physiology, including growth and stress resistance.

Results

Increased respiration dependence is associated with a missense PYK variant

Treating aerobic glycolysis as a complex, quantitative trait, we assessed the amount of residual respiration on glucose-rich media across a set of genotypically and phenotypically diverse wild *S. pombe* isolates. Resistance to antimycin A, which blocks the respiratory chain by inhibiting ubiquinol-cytochrome c oxidoreductase[42], was used as a proxy readout for cellular dependence on oxidative phosphorylation. The standard laboratory strain *972 h*$^{-}$ shows a moderate reduction in maximum growth rate and biomass yield in this condition[29,43]. We applied a colony-based assay to determine relative fitness of each strain in rich glucose media with and without antimycin A. The resulting resistance scores showed a large diversity between strains (Fig. 1A, Supplementary Fig. 1, Supplementary Table 1). Notably, the laboratory strain was among the most sensitive (score=1, rank=10 of 154), while the mean score was 1.25±0.15 for all strains tested.

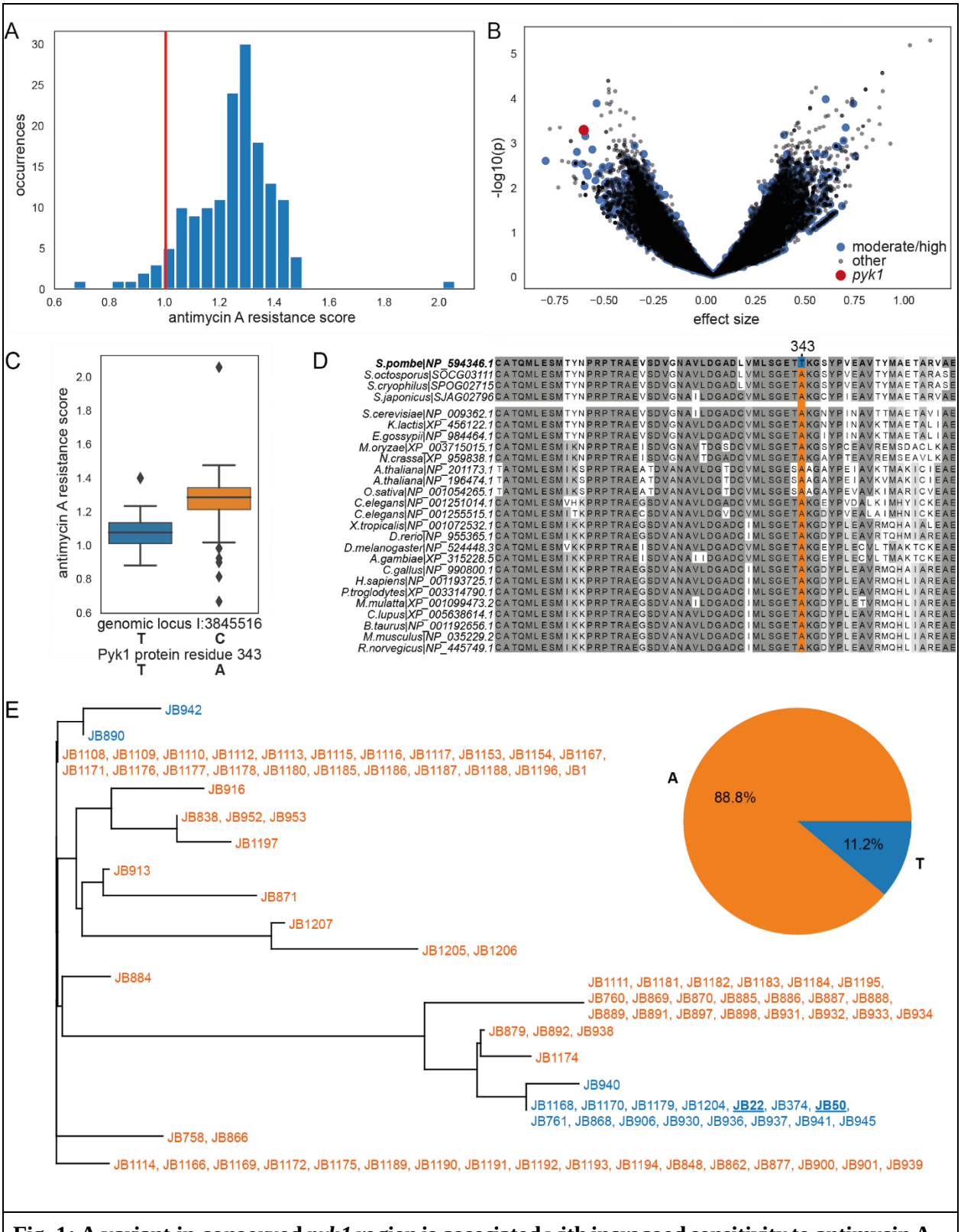

Fig. 1: A variant in conserved *pyk1* region is associated with increased sensitivity to antimycin A. **(A)** Distribution of antimycin A resistance scores for wild isolates, compared to standard laboratory strain (red vertical line). Resistance scores are the ratio of fitness on rich glucose media with *vs* without 500 μg/L antimycin A. Fitness was estimated based on colony size on solid media, corrected for spatial and plate effects (Methods). After quality control, we obtained quantitative fitness scores for 154 strains, with a signal-to-noise ratio of 29.8 and an unexplained variance of 0.12. **(B)** Volcano plot of a genome-wide association using mixed-model linear regression of antimycin A

resistance for 118,527 genetic variants. Variants with moderate or high impact are shown in blue. Red dot: the variant at locus I:3845516, which causes a T343A change in the Pyk1 amino-acid sequence. This variant was among the top scoring (effect size=-0.645, rank 34; p=0.0008, rank 70).
(C) Boxplot showing antimycin A resistance grouped by the two alleles at the *pyk1* locus.
(D) Sequence alignment of the region of interest in eukaryotic PYK proteins. The threonine residue at the highlighted position 343 is unique for the reference (laboratory) *S. pombe* strains. For this analysis, we collected 25 Pyk1 homologues from a wide variety of eukaryotes, including animals, plants and fungi, using the HomoloGene resource (Accession 37650). We manually expanded the homologous group to include three other species of the *Schizosaccharomyces* genus[44]. Sequences were aligned with MAFFT[45] and visualised with Jalview[46].
(E) Phylogenetic tree based on 31 biallelic SNPs in *pyk1* and in 500bp up- and down-stream regions. Strains carrying the common A-allele are in orange, while strains carrying the unusual T-allele are in blue (strain names as in ref. [32]). Strains JB22 and JB50 (underlined and bold) refer to heterothallic and homothallic versions of the laboratory strain, respectively. The pie chart shows the relative allele frequencies at the genomic locus across all wild strains. Genotype calls at the locus were checked manually and were conclusive, i.e. no strain produced reads with both alleles.

The antimycin A resistance trait showed an estimated narrow-sense heritability of 0.54, which is substantially higher than for most of the 223 phenotypes previously reported[32]. This result indicates a strong genetic basis for the dependence on respiration. We performed a genome-wide association study (GWAS) to identify loci linked to resistance among 118,527 small genetic variants, including single-nucleotide polymorphisms (SNPs) and small insertions or deletions (Fig. 1B). Compared to a recent GWAS in budding yeast[47], our statistical power was lower, partly due to the low number of strains and the strong population substructure[32]. We therefore manually assessed the associated variants, based on p-value, effect size, and literature. Among the top-100 associations (by p-value, Supplementary Table 2), eight were predicted to have moderate or high impact as defined by SnpEff[48], and six of those were located in genes with functional annotation in PomBase[49]. Two of these six variants were in *S. pombe* specific genes: *wtf16* and *wtf8*[50]. Other variants were in *ubp9*, encoding a ubiquitin C-terminal hydrolase, in *pfl5*, encoding a cell-surface glycoprotein, and in *jac1*, encoding a mitochondrial 2Fe-2S cluster assembly co-chaperone. One missense variant caught our particular attention: this SNP was among the top scoring (Fig. 1B) and leads to a T343A amino-acid sequence change in Pyk1, encoding the single PYK in *S. pombe.* Strains with a threonine residue at position 343 ('T-allele') showed a median resistance score of 1.07, while strains with an alanine ('A-allele') showed a ~15% higher median resistance of 1.28 (Fig. 1C).

An analysis of 26 PYK protein sequences from diverse eukaryotes revealed strong conservation, showing 45-93% agreement with the consensus sequence called from the alignment (Fig. 1D). The threonine residue in the reference (laboratory) strain of *S. pombe* was unique in this highly conserved region of all PYK sequences. All other species featured an alanine residue at this position, including three other *Schizosaccharomyces* species (Fig. 1D). The reference allele (T-allele) in the laboratory strain is the minor allele in our strain collection, found only in 18 of 161 strains (Fig. 1E). The rare T-allele occurred in four unique sequences in the phylogenetic tree, split up over two highly divergent lineages (Fig. 1E). This result was confirmed by considering a consensus tree based on the entire genome[32]. For 10 of the 18 T-allele strains, the geographical origin is known, with most being isolated in Europe but also one each from Asia and Australia. The substrate is predominantly

fermenting grapes (as for most other strains), and one each from lychee and glace syrup, which reflects the fact that most *S. pombe* strains have been isolated from human-created niches. We conclude that the T-allele at position 343 is a rare, naturally occurring allele, which appears to have arisen, and been maintained, independently in two distant lineages.

Replacing the *pyk1* allele in laboratory strain leads to higher PYK activity and metabolic reprogramming

Many species possess two or more PYK isozymes with different activity and/or expression patterns. In *S. cerevisiae*, the minor isozymes can complement for the loss of the major isozymes[51]. The *S. pombe* reference genome[52], based on the laboratory strain *972,* features only one PYK isoform. To test whether this is also the case for the other strains, we searched the *de novo* assemblies of each wild strain genome[32] with tblastn[53] for Pyk1 homologues. This search consistently produced a single hit only (Pyk1 itself).

We set out to analyse the effect of the *pyk1* SNP on cellular metabolism. Using seamless CRISPR/Cas9-based gene editing[54], we replaced the *pyk1* T-allele in the laboratory strain for the more common A-allele. We introduced the A-allele in both a heterothallic h^- and a homothallic h^{90} laboratory strain, without any other genetic perturbations. We then selected three independently edited strains for both h^- and h^{90} backgrounds to use as biological replicates throughout this study. Below, we use the abbreviations 'T-strain' for the normal laboratory strains and 'A-strains' for the edited $pyk1^{T343A}$ h^-/h^{90} strains. These strains allowed us to study the impact of the *pyk1* SNP in a controlled and well-characterized genetic background.

It has been reported that *S. pombe* features lower PYK activity than *S. cerevisiae*[41,55]. This conclusion was however derived from the laboratory strain, which contains the unusual *pyk1* allele. To investigate the impact of the *pyk1* SNP on metabolism, we applied a targeted metabolomics workflow based on liquid chromatography - selective reaction monitoring (LC-SRM). We quantified key metabolites potentially affected by PYK activity[56,57], including glycolytic, pentose-phosphate pathway and citric-acid cycle intermediates as well as redox cofactors and adenine nucleotides. Data was obtained for nine replicates of the T-strain and eight replicates of the A-strain (Fig. 2A-D, Fig. 3, Supplementary Table 3, Supplementary Fig. 2). Technical replicates sampled from the same culture, but prepared and measured separately, were highly correlated (Pearson r=0.93), indicating that our workflow is robust and that most of the observed variation is biological. Over the entire data set, the median coefficient of variation was 17.2%. A principal component analysis (PCA) of metabolite data distinguished all strains based on the SNP in *pyk1* (Fig. 2A).

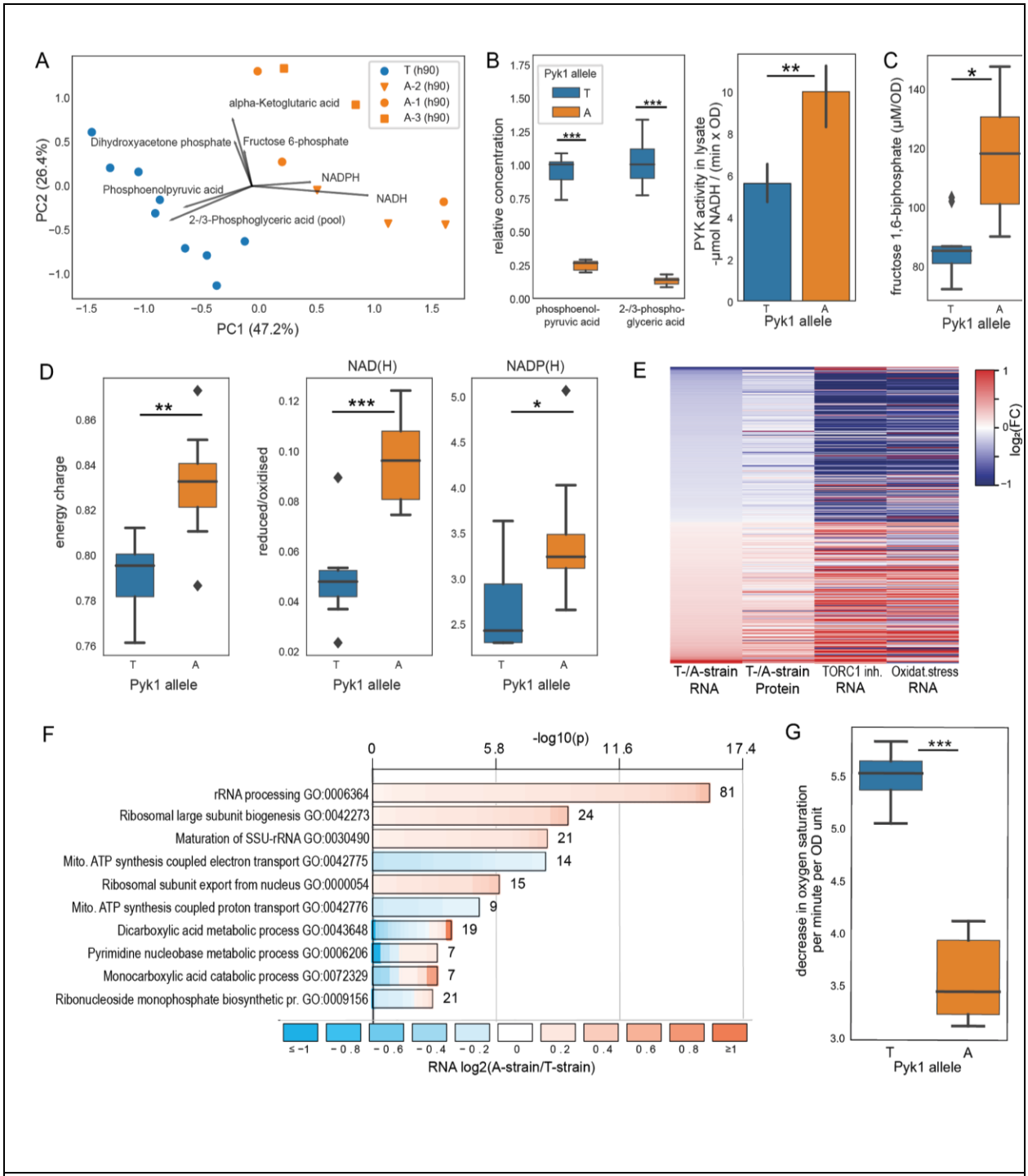

Fig. 2: Multi-omic functional investigation of Pyk1 variants.

(A) PCA of metabolite data based on concentrations of 27 central-carbon metabolism intermediates. To visualise this high-dimensional data set, we divided the concentration of each metabolite by the median concentration of the T-strain. This normalisation corrects for the large differences in concentrations observed between metabolites but maintains the relative variance within each metabolite. Biological replicates of the T- and A-strains show distinct profiles, largely driven by concentrations of phosphoenolpyruvate, 2-/3-phosphoglyceric acid, NADH and NADPH, as indicated by top loading vectors for each principal component. The biological repeats for the three edited A-strains (circles, squares and triangles) behave similarly, with a variance comparable to that of the biological replicates of the single T-strain.

(B) Left boxplot: two glycolytic intermediates directly upstream of PYK were strongly depleted in the

A-strain. Right barplot: PYK activity was directly measured using a lactate dehydrogenase-coupled colorimetric enzyme activity assay, showing the mean and standard deviation of substrate conversion rate for 3 biological replicates measured in technical duplicates each. Significance keys: * $p<0.05$, ** $p<0.005$, *** $p<0.0005$ (Welch's t-test).
(C) Concentrations of fructose-1,6-bisphosphate, which correlate with glycolytic flux, are significantly higher in A-strain (ratio = 1.35).
(D) Boxplots for selected metabolomics data indicate differences in energy and redox status between T- and A-strains.
(E) Heatmap of the 432 genes that are differentially expressed at the RNA level between the T- and A-strains (FDR <10%) and are measured in all four conditions (columns). First column: genes ordered by increasing fold-changes for RNAs (computed as $\log_2$[T]-$\log_2$[A]). Second column: fold-changes for proteins (computed as $\log_2$[T]-$\log_2$[A]). Third column: fold-changes for RNAs in cells treated with rapamycin & caffeine (TORC1 inhibition; computed as $\log_2$[treatment]-$\log_2$[control]) (data from ref. [58]). Fourth column: fold-changes for RNAs in cells treated with H_2O_2 (oxidative stress; computed as $\log_2$[treatment]-$\log_2$[control]) (data from ref. [59]). Log2 fold-changes are capped at absolute values of 1 for all columns.
(F) Gene Ontology (GO) enrichment analysis of differentially expressed transcripts (using all measured transcripts as background). Shown are Biological Process terms only, with additional plots for Molecular Function and Cellular Component terms in Supplementary Fig. 3. The length of the bar represents the significance of the enrichment, while its color reflects the direction and magnitude of differential expression (A- *vs* T-strain) of individual genes annotated to this term.
(G) Boxplot of oxygen consumption rates in A- and T-strains (ratio of means=0.65, $p=1.31\times10^{-5}$, Welch's T-test, 3 biological replicates, each measured in technical duplicates).

We observed a strong depletion of glycolytic intermediates upstream of PYK, with mean levels of phosphoenolpyruvate and 2-/3-phosphoglyceric acid in the A-strains only 25.9% and 12.7% of those in the T-strain (Fig. 2B, p_{adj}=8.7x10-8 and 3.7x10-6, Welch's t-test, Benjamini-Hochberg corrected). This result suggests that the A343T mutation reduces the activity of the Pyk1 enzyme. We directly tested this hypothesis by determining PYK activity in lysates of 3 biological replicates each of the A- and T-strain grown in rich glucose media, using a lactate dehydrogenase-coupled photometric assay in technical duplicates. With a buffer composition similar to those previously used[60], the A-strains showed a 78.1% higher activity compared to the T-strain (p=0.0023, Welch's t-test) (Fig. 2B).

The metabolomics data also allowed us to estimate several physiological parameters. The A-strains exhibited significantly higher levels of the flux-signalling metabolite[61] fructose 1,6-bisphosphate (ratio 1.35, p_{adj}=0.015) (Fig. 2C). The levels of this metabolite are known to strongly correlate with glycolytic flux in several yeast species[62,63], consistent with a higher flux in the A-strain. Furthermore, cellular energy charge[64] was 4.7% higher in the A-strains (Fig. 2D; p=0.002, Welch's t-test). These values are within the range reported for other organisms[65]. We used the ratio of the reduced to oxidised forms of NAD(H), NAD(P)H and L-glutathione as readouts for cellular redox status (Fig. 2D). For NAD(H), the A-strains showed an increase from 0.048 to 0.096 (p=0.0001, Welch's t-test). The same pattern was evident for NADP(H), where the median ratio was 3.24 in the A-strains, but only 2.43 in the T-strain (p=0.024). The A-strain had a significantly higher concentration of the reduced isoform of L-glutathione (ratio 1.30, p_{adj}=0.015, Welch's t-test, Fig. 2D), but no significant difference was apparent in the ratio of the reduced to oxidised isoforms, where the median for the A-strains was 2.01 *vs* 1.89 for the T-strain (p=0.289, Welch's t-test). These results are in line with the paradigm that NADH/NAD+ ratios are maintained at low levels to maximise availability of

electron acceptors for catabolic processes, while NADPH/NADP+ ratios are maintained at high levels to provide electrons for anabolic processes and the antioxidant response[66]. As part of the antioxidant defence, which includes glutathione-, peroxiredoxin- and thioredoxin-dependent reduction systems, NADPH is limiting when cells are challenged with oxidative stress[67–70]. While analytical methods cannot distinguish between different compartments or sub-populations of these cofactors[71], and our sample extraction method may allow some interconversion between reduced and oxidised isoforms[72], these findings are consistent with the hypothesis that the A-strain respires less and thus has a lower oxidative burden.

Increased PYK activity leads to transcriptome and proteome changes reflecting increased fermentation and decreased respiration

To further analyse the effects of the *pyk1* SNP, we characterised the transcriptomes and proteomes of the T- and A-strains using RNA-seq and mass spectrometry, respectively. We could quantify 7750 transcripts (including non-coding RNAs) and 3234 proteins in both strains, allowing for a broad analysis of genome regulation. The expression of *pyk1* itself was similar in the T- and A-strains at both the transcript (log_2[fold change]=0.016, p_{adj}=0.91) and protein level (log_2[fold change]=-0.001, p_{adj}=0.94). This result means that the differences between the two strains were not caused by changes in *pyk1* expression. Notably, the *pyk1* allele replacement led to substantial changes in both the transcriptome and proteome. Overall, 960 transcripts and 434 proteins were differentially expressed between the T- and A-strains, at a false-discovery rate (FDR) of ≤10%. While changes at the transcriptome and proteome levels generally correlated well (r=0.65 for all genes with differentially expressed transcripts and/or proteins), we also found a large number of genes to be regulated exclusively on the protein level (Supplementary Fig. 5). These proteins were enriched in functions related to cytoplasmic translation and depleted in functions related to ribosome biogenesis (Supplementary Tables 5 and 6). This result raises the possibility that post-transcriptional gene regulation plays an important role in controlling translation.

The differentially expressed genes were enriched in functions related to respiration and energy-demanding processes, like translation and ribosome biogenesis. These enrichments were evident at both the level of the transcriptome (Fig. 2F, Supplementary Fig. 3) and proteome (Supplementary Fig. 4). Transcripts encoding respiratory chain and oxidative phosphorylation proteins were more highly expressed in the T-strain (Fig. 3), while those related to ribosome biogenesis and rRNA processing were more highly expressed in the A-strain. Some functional terms (e.g., NAD-binding) contained genes that were strongly regulated in either direction. Several of the most differentially expressed transcripts and proteins were directly involved in pyruvate metabolism (Fig. 3). The *mae2* gene was most strongly regulated at both transcript and protein levels, being more highly expressed in the T-strain. Mae2 is an enzyme that catalyses the reaction from malate and oxaloacetate to pyruvate[73]. Thus, the T-strain may up-regulate Mae2 to replenish pyruvate using an alternate way that is largely independent of glycolytic flux. The *pdc101* and *atd1* genes, on the other hand, were expressed more highly in the A-strain. These genes encode pyruvate decarboxylase and aldehyde dehydrogenase, respectively, and their induction is consistent with higher glycolytic flux and increased fermentation[29]. These expression changes are consistent with the central role of PYK in glycolysis and the observed metabolic effects mediated by the Pyk1 variants.

The target of rapamycin complex 1 (TORC1) signalling pathway controls energy metabolism and promotes aerobic glycolysis in response to cellular nutrients[2]. Enrichment analysis using AnGeLi[74] revealed substantial overlaps between the differential expression signature of the T- and A-strains and the signature of TORC1 inhibition (Fig. 2E)[58]: 58 transcripts and 33 proteins induced by TORC1 inhibition were more highly expressed in the T-strain ($p=6.1x10^{-12}$ and $4.1x10^{-7}$, respectively), while 118 transcripts and 72 proteins repressed by TORC1 inhibition were more lowly expressed in the T-strain ($p=1.8x10^{-59}$ and $2.1x10^{-30}$, respectively). Thus, the expression signature of the T-strain resembles the signature caused by TORC1 inhibition, which leads to reduced glycolysis. Moreover, genes induced in response to oxidative stress were also differentially expressed; examples include *gpx1,* encoding glutathione peroxidase, and *grx1,* encoding glutaredoxin. Accordingly, the differential expression signature between the T- and A-strains also showed substantial overlaps with the core environmental stress response triggered by oxidants and other stresses (Fig. 2E)[59]: 63 transcripts induced by oxidative stress were higher expressed in the T-strain ($p=7.0x10^{-4}$), while 149 transcripts and 94 proteins repressed by stress were lower expressed in the T-strain ($p=2.8x10^{-68}$ and $1.4x10^{-37}$, respectively. Thus, the expression signature of the T-strain also resembles the general signature of cells exposed to different types of stress, likely reflecting the higher load of reactive oxygen species from respiration. Together, the observed gene-expression reprogramming suggests that the T-strain features higher respiration and pentose-phosphate pathway activity (Fig. 3). Similarly, budding yeast strains genetically engineered to alter PYK activity reconfigure their metabolism, with a reduced activity leading to higher respiration (to meet energy demands) and pentose-phosphate metabolism (to increase reducing agents required to detoxify reactive oxygen species produced by respiration)[34].

To independently confirm the shift from respiration to fermentation in the A-strain, we measured oxygen consumption in rich glucose media. Indeed, the A-strain consumed oxygen at a 34.1% lower rate than the T-strain (Fig. 2G). This result supports the prediction that the A-strain respires at lower levels than the T-strain. We conclude that the *pyk1* allele replacement is sufficient for a systemic regulatory shift from respiration to fermentation in the A-strain, which is apparent by key metabolome changes and in turn is supported by adjustments in the transcriptome and proteome (Fig. 3).

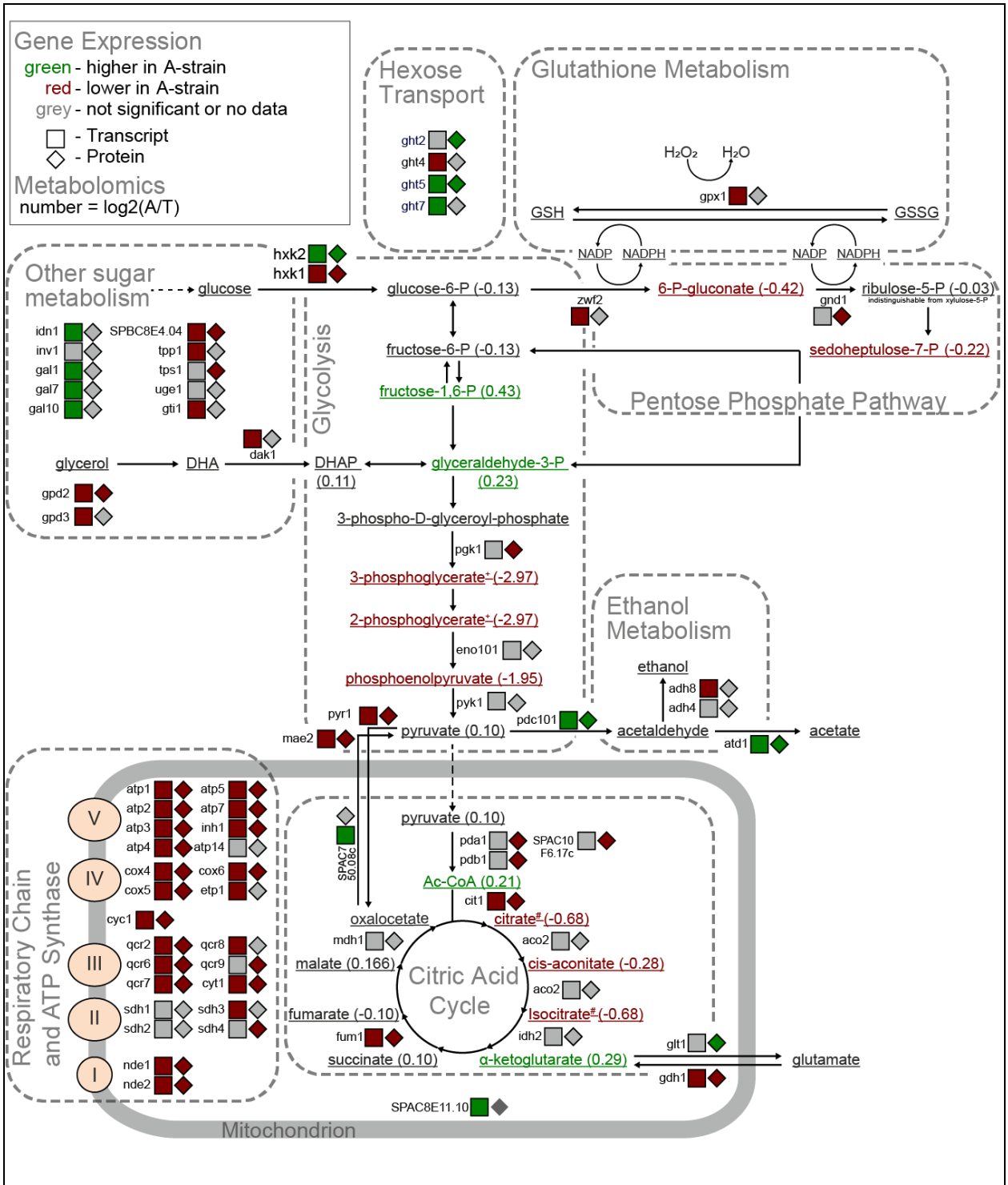

Fig. 3: Metabolic network showing metabolome, transcriptome and proteome changes triggered by *pyk1* allele replacement. Metabolites, transcripts and proteins are coloured by their abundance ratios in A-strain relative to T-strain (see legend top left for details). For clarity, enzymes without protein or transcript changes are not shown (e.g. most upper glycolysis). Two metabolite pairs are indistinguishable by our method (marked as '+' and '#)'.

Increased glycolytic flux affects cellular growth, lifespan, and stress resistance

Given the metabolic and gene-expression changes associated with the *pyk1* allele replacement, we expected that the A-strain will feature phenotypic changes at the cellular level. We therefore interrogated diverse cellular traits. We confirmed that the T-strain was more sensitive than the A-strain to inhibition of respiration by antimycin A (Fig. 4A), which supports the prediction from the GWAS. We then recorded growth curves for A- and T-strains. The A-strain showed a ~20% higher maximum growth rate than the T-strain during proliferation in rich glucose media (Fig. 4B). Thus, the SNP in *pyk1* has a pronounced inhibitory effect on cell proliferation in the standard laboratory strain under a standard growth condition.

A natural SNP in a key metabolic enzyme could differentially affect fitness on different carbon sources. While the A-strain grows more rapidly on glucose, the T-strain might have fitness advantages in other conditions. To test for such a trade-off, we tested 12 common carbon sources in four different base media (Fig. 4C and Supplementary Table 7). Both strains showed rapid cell growth on glucose, fructose and sucrose, intermediate growth on raffinose, mannose and maltose, and slow growth on the other carbon sources. Consistent with the result in Fig. 4B, the A-strain grew faster than the T-strain on the fermentable carbon sources glucose, fructose and sucrose. In the other carbon sources, the two strains showed similar growth. Thus, the T-strain did not show increased fitness in any of the tested conditions (Fig. 4C). We also tested for differential growth of the A- and T-strains on different nitrogen sources. Both strains showed substantial growth on 54 of the 95 nitrogen sources (Fig. 4D and Supplementary Table 8). The A-strain grew about 2-fold better than the T-strain on L-phenylalanine but worse on L-cysteine. Validation by spot assays on solid media, however, could only confirm the difference for phenylalanine (Fig. 4F). In conclusion, these broad phenotypic assays did not provide support for the idea that the T-allele might represent an adaptation to specific carbon or nitrogen sources.

Only a fraction of natural environments might enable rapid proliferation as in the laboratory. Thus, resistance to stress could be a more important selection factor in determining fitness. Trade-offs are a key concept in evolutionary adaptation[75], and microbes show an anti-correlation between growth rate and stress resistance[76,77]. In budding yeast, artificially reduced glycolytic flux leads to increased resistance to oxidative stress[34], and mammalian cells show a similar feature[78]. We therefore assessed the ability of the A- and T- strains to endure oxidative stress triggered by hydrogen peroxide (H_2O_2) or diamide. Indeed, the T-strain was substantially more resistant to both oxidants than the A-strain (Fig. 4A). Oxidative stress is a byproduct of cellular respiration, and the T-strain may feature a higher basal protection from oxidative stress due to higher respiratory activity. This protection is consistent with our observation that core environmental stress response genes were more highly expressed in the T-strain. The environment can also be a source of oxidants, e.g. in microbial communities with H_2O_2 producing lactic acid bacteria[79,80]. Thus, a natural SNP promoting oxidative-stress resistance may be beneficial. We conclude that the slower growth of the T-strain, compared to the A-strain, is offset by an increased resistance to oxidative stress. Both traits may be systemic properties emerging from the up-regulation of respiration at the cost of fermentation, triggered by the T-allele.

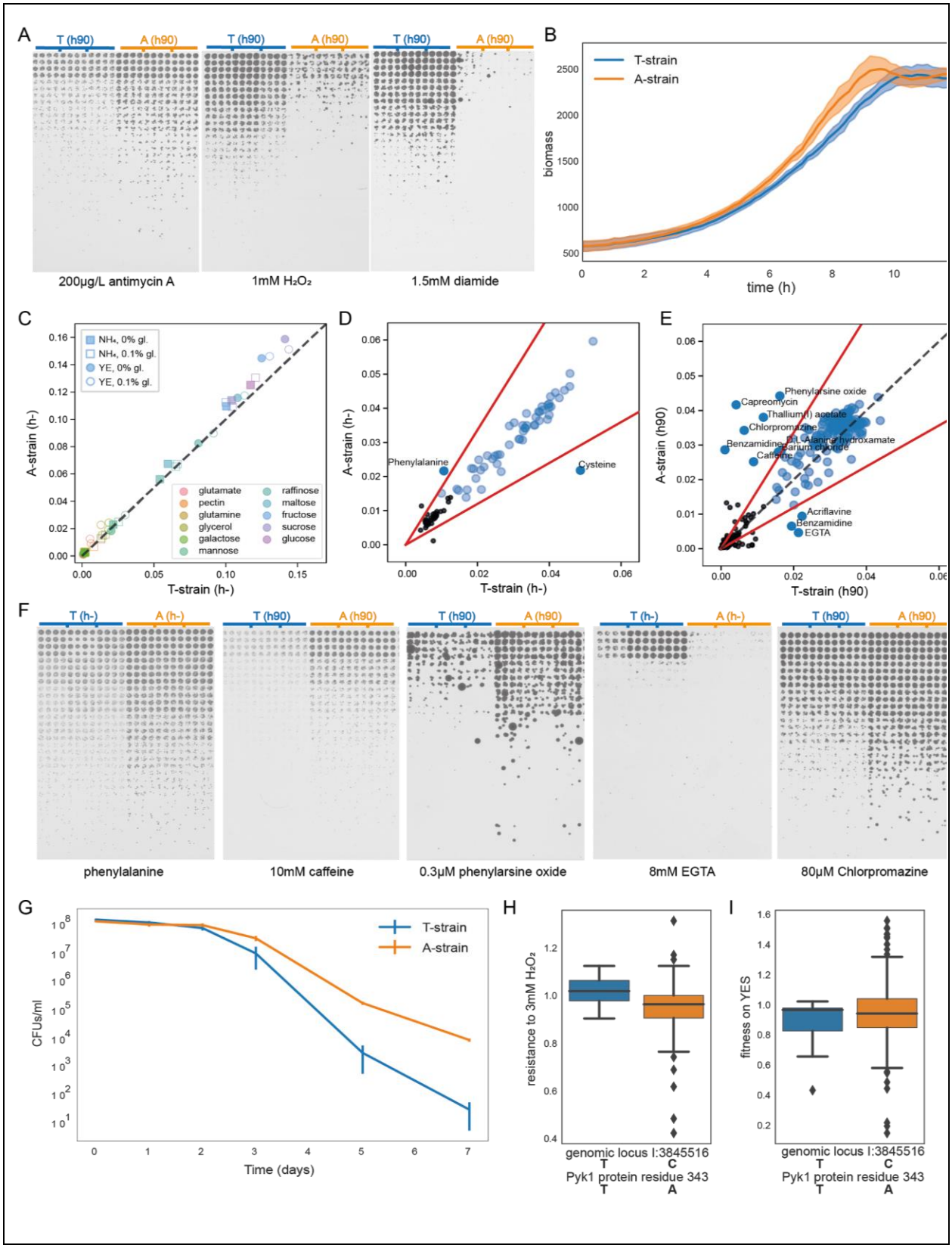

Fig. 4: Cellular phenotypes mediated by *pyk1* allele replacement.
(A) Spot assays on solid media from a three-fold dilution series of exponential cultures at the same cell density in 96-well plates (3 biological replicates of each strain) and spotted in 16 technical replicates (each dilution in 4x4 square). The A-strain is more resistant to antimycin A but less resistant to oxidative stress triggered by H_2O_2 or diamide.

(B) Growth curves of A- and T-strains in rich glucose media. The dark lines show the means, and the shaded areas represent the standard deviations. The maximum slope of growth curves was 423.7±48.8 biomass units per hr (mean±standard deviation) for A-strain compared to 351.9±25.1 for T-strain, a difference of 20.4% (6 biological repeats each from separate pre-cultures, p=0.0136, Welch's t-test).
(C) Fitness (approximated by maximum slope of smoothed growth curves) of A- and T-strains on 12 carbon sources, with either yeast extract (YE) or ammonium (NH_4), with or without 0.1% priming glucose to support initial growth. For all 48 conditions, two biological replicates of A- and T-strains were grown in technical quadruplicates each.
(D) Fitness of A- and T-strains on 95 nitrogen sources on Biolog Phenotype MicroArrays. Conditions with no substantial growth were excluded (black circles, maximum slope <0.015). Red lines show arbitrary significance cut-off, put at $|\log_2(\text{A-strain/T-strain})|>0.75$.
(E) Fitness of A- and T-strains on 72 different drugs and toxins, at 4 concentrations each, on Biolog Phenotype MicroArrays. Graph details and cut-off as in (D). (Results for benzamidine were inconclusive, with both strains comparatively resistant in one concentration each.)
(F) Spot assays as in (A) to validate selected results from (C) and (D).
(G) Chronological lifespan of A- and T-strains, i.e. the proportion of non-dividing cells in stationary phase that maintain proliferative potential after refeeding. The data show colony forming units (CFUs) per ml of culture over 7 days of stationary phase in glucose-depleted rich media. Three biological repeats were carried out for both strains, with each repeat measured as technical triplicates. Error bars represent standard deviations.
(H) Boxplot showing resistance to 3mM H_2O_2 grouped by *pyk1* allele for 156 strains from our collection. The T-strains had a higher mean fitness in H_2O_2 than the A-strains (1.01±0.06 *vs* 0.95±0.11; p=0.0021, Welch's t-test). The resistance score was obtained as for antimycin A.
(I) Boxplot showing growth fitness on rich media, grouped by *pyk1* allele for 158 *S. pombe* strains (0.88±0.16 *vs* 0.94±0.24; p=0.18, Welch's t-test).

We wondered whether the T-strain might feature fitness advantages in conditions other than oxidative stress. To this end, we screened for differential growth of the A- and T-strains on 72 different drugs and toxins. The strains appeared to be differentially sensitive to 9 compounds (Fig. 4E). The A-strain was more resistant to barium chloride, D-L-Alanine hydroxamate, caffeine (pleiotropic effects, including TOR inhibition)[58], chlorpromazine (causes membrane stress)[81], capreomycin (binds to ribosomes)[82] and phenylarsine oxide (inhibitor of tyrosine phosphatases)[83]. Notably, the A-strain was also more resistant to thallium (I) acetate, which is highly toxic due to its similarity to potassium ions and binds to mammalian PYK with a stronger affinity, but weaker activating effect, than potassium[84,85]. The T-strain, on the other hand, was more resistant to acriflavine, an antiseptic, and EGTA, a chelator of bivalent cations (including Mg^{2+} which activates *S. cerevisiae* PYK[86]). We manually inspected dose-response curves (Supplementary Fig. 6) to select four compounds for validation based on overall difference in maximum growth rate and consistency across concentrations. Using spot assays, we could validate the differential sensitivity to all selected compounds: caffeine, phenylarsine oxide, EGTA, and chlorpromazine (Fig. 4F). It is striking that the *pyk1* SNP differentially affected the resistance to this broad range of stresses, suggesting a general role of glycolysis in stress resistance beyond the known role in oxidative stress.

The existence of a fundamental link between metabolism and lifespan is well known, e.g. through the observation that dietary restriction extends lifespan from yeast to humans[87]. In various model systems, increased respiration[30,88–90] and slower growth[91–94] correlate with increased lifespan. We therefore expected the T-strain to be longer lived than the A-strain

and measured the chronological lifespan of both strains. Surprisingly, the A-strain was longer-lived, with a mean viability of 25.3% after 3 days, compared to 6.5% for the T-strain (Fig. 4G). Reduced glycolytic flux has been reported to shorten replicative life span in budding yeast[95]. We therefore speculate that unrestricted glycolytic flux generally promotes longevity, but mechanistic processes involved will require further investigation.

Our findings show that the *pyk1* SNP has substantial effects on growth rate and oxidative-stress resistance in the genetic background of the standard laboratory strain. Are such effects generally evident in other strain backgrounds? To address this question, we measured oxidative-stress resistance and growth rates for all wild strains. Indeed, the T-allele was significantly associated with higher resistance to H_2O_2 (Fig. 4H). With respect to growth rate, on the other hand, no significant difference was evident between strains containing the T- or A-alleles (Fig. 4I). These results suggest that the *pyk1* SNP can play a substantial role in oxidative-stress resistance, while growth rate may be a more complex trait, which is controlled by many other loci or buffered by counteracting mutations.

Discussion

Many eukaryotes, from budding yeast to humans, possess low- and high-activity PYK isozymes. PYK activity has been implicated in coordinating fermentation with respiration in synthetic *S. cerevisiae* models[34,35]. The low-activity isoform of *S. cerevisiae* is expressed under respiratory growth conditions[51]. Using an unbiased, genome-wide approach, we identified a naturally occurring SNP in the sole *S. pombe* PYK gene. Our findings show that this SNP affects PYK activity and glycolytic flux and is sufficient to cause a shift in the respiration-fermentation balance. When we replaced the T-allele of the laboratory strain with the common A-allele, which is broadly conserved in most *S. pombe* strains all other eukaryotes examined, glycolytic flux increased and oxygen consumption decreased.This metabolic re-programming led to changes in gene expression at the transcriptome and proteome levels, resembling the signatures of rapidly proliferating cells with high TORC1 activity and no stress exposure. At the cellular level, the allele replacement led to increased growth and chronological lifespan but decreased resistance to oxidative stress. Cellular growth and stress resistance are linked with gene regulation, although cause-effect relationships are not really understood[77,96–100]. The extraordinary plasticity in response to altered glycolytic flux, triggered by a single-nucleotide change, highlights the fundamental impact of the glycolysis on cellular control, physiology and adaptation. Possessing only a single PYK isoform, *S. pombe* is unlikely to have a pre-existing genetic or signalling programme for the regulation of high- and low-activity PYK states. Yet, a mutation in Pyk1 that changes its activity is sufficient to induce coherent metabolic, regulatory and cellular responses. A PYK-induced change in glycolytic flux is hence the cause, not a consequence, of major changes in cell regulation and physiology.

What might be the evolutionary and ecological role of the *pyk1* SNP? We propose that the mutation in the laboratory strain is beneficial given its maintenance at a strongly conserved position, its occurrence in two independent *S. pombe* lineages, its associated phenotypes, and the use of low-activity isoforms in other organisms. The literature suggests that low PYK activity could help cells to retain more carbon intermediates for biosynthesis[101–103]. Our

results, and other recent research[104], do not support this hypothesis as cells with low Pyk1 activity grow slower and form less biomass. Our phenotypic assays also do not support the possibility that the *pyk1* SNP is adaptive on specific carbon or nitrogen sources. However, we have identified several stress conditions where the laboratory strain exhibits higher fitness than the allele-replacement strain, most notably oxidative stress. It is plausible that stress resistance has provided the selection factor for the low-activity Pyk1 allele. Accordingly, we propose that altered stress tolerance provides a biological rationale for the evolution of systems that allow conditional switching between high- and low-activity PYK isozymes.

Methods

Wild strain phenotyping and GWAS

We constructed two arrays of 384 strains, each containing a reference grid of 96 JB22 colonies (standard laboratory strain 972), around which 159 wild isolates from our collection[32] were randomly arranged in triplicates, with additional internal, interspersed JB22 controls. A RoToR HDA pinning robot (Singer Instruments) was used to copy the arrayed strains onto various growth media. Plates were grown for 2 days at 32°C, and images were acquired by transmission scanning (Epson V800 Photo). Colony sizes were determined with *gitter*[105] and corrected for spatial biases using reference-grid normalisation[106], as implemented in our freely available pipeline (github.com/Bahler-Lab/pyphe-slim). Further, strains which did not grow at all (colony size <10 pixels at 600 dpi scanning resolution) or showed abnormal circularity values (>1.1 or <0.85) were excluded from further analysis. Strains for which no consistent fitness estimate could be obtained were also excluded (standard deviation of triplicates greater than standard deviation of all colonies of all strains), which removed two strains from our data set. For the rest, individual corrected colony sizes were averaged and condition-specific resistance/fitness scores were determined by dividing the corrected colony size in the condition of interest by that of the control condition without drug. Signal to noise ratios were determined by dividing the mean fitness of the internal controls by their standard deviation. The fraction of unexplained variance was determined by dividing the standard deviation of the internal controls by that of the entire dataset.

For GWAS, phenotype values were transformed to normal shape using the Box-Cox method, mean-centred at zero and normalised to unit variance, using PowerTransformer of *scikit-learn*[107]. Genomic variants were called from published and aligned sequence data[32] using *freebayes*[108], with the following options: --ploidy 1 --standard-filters --min-coverage 10 --min-alternate-count 3. The version of the reference genome used was ASM294v2. SNPs within 3bp of an indel were filtered out using the --SnpGap option of *bcftools*[109]. Low quality calls and loci where >50% of the population was not genotyped were removed using the --max-missing 0.5 --minQ 30 --remove-filtered-all options of *vcftools*[110]. Variant effects were predicted using SnpEff[48]. Variants were filtered for a minor allele frequency of >5% and converted to plink format using *plink*[111]. A kinship matrix was constructed in LDAK5[112,113] by first cutting and thinning predictors, then calculating their weights, and finally using the direct method for obtaining the kinship matrix. All steps used default options. Heritability estimates

were obtained by REML as implemented in LDAK5. Linear mixed model association was performed in LDAK5, using the previously generated kinship matrix to correct for population structure.

Phylogenetics

The phylogenetic tree in Fig. 1 was constructed by filtering biallelic SNPs in the region ±500bp around the *pyk1* gene (I:1:3844243-3847145) using *bcftools*. This vcf was converted to a pseudo alignment in fasta format with *VCF-kit*[114]. The tree was constructed by the neighbour-joining method, implemented in *ClustalW2*[115], accessed through the EBI web-interface[116], and drawn in seaview[117].

Construction of allele replacement strains

The allele replacement strains were generated using the CRISPR-Cas9 system. The plasmid containing the gRNA targeting the *pyk1* SNP in *968 h*[90] (homothallic) and *972 h*[-] (heterothallic) was generated as described[54] using the following primers: gRNA.JB50-F: GCTTTCCGGTGAGACTACCAgttttagagctagaaatagc and gRNA.JB50-R: TGGTAGTCTCACCGGAAAGCttcttcggtacaggttatgt
Proper gRNA cloning was assessed by Sanger sequencing. The template for homologous recombination was generated using the following primers (underlined is the point mutation introduced in the T strain to convert it to the A strain):
HR_JB50-F:
ACCCTCGTCCTACTCGTGCCGAGGTTTCCGATGTTGGTAACGCCGTTCTCGATGGTGC
TGACTTGGTCATGCTTTCCGGTGAGACTGCCAAGGGTTCTTA
HR_JB50-R:
GTAAGGGATGGAAGCCTCAGCAACACGGGCAGTCTCAGCCATGTAGGTAACGGCTTCA
ACGGGGTAAGAACCCTTGGCAGTCTCACCGGAAAGCATGACC
The following primers were used to identify and confirm successful mutants, of which three were kept and used for experiments in order to reduce the risk of observing the effects of off-target mutations:
Pyk1ck-F: GATGTTGGTAACGCCGTTCT
Pyk1ck-R: GGACGGTACTTGGAGCAGAG

Cell culture for multi-omics experiments

Transcriptomes and proteomes were measured from the same cell culture, in five biological repeats per strain. Strains were woken up on yeast extract with supplement (YES) agar and incubated for two days at 32°C. Then, 50ml pre-cultures (YES medium, 32°C, 170 rpm) were grown overnight and used to inoculate 200 ml cultures (YES medium) at an OD_{600} of 0.1 These cells were then grown until OD_{600} of 0.8 and harvested as described below.

Transcriptomics experiments

When cells reached OD 0.8, 25 ml were collected by centrifugation and snap frozen in liquid nitrogen. RNA was extracted with a hot phenol method described[118]. RNA was further purified with Qiagen RNAeasy columns, and DNAse treatment was performed in the columns (as suggested by manufacturer) prior to library preparation. RNA quality was assessed with a Bioanalyzer instrument (Agilent), and all samples presented a RIN (RNA Integrity Number) >9. cDNA libraries were prepared with the Illumina TruSeq stranded

mRNA kit, according to the manufacturer's specifications, by the Cologne Centre for Genomics (CCG) facility. The samples were sequenced on a single lane of an Illumina Hiseq4000 to produce 2x75nt reads.

Reads were trimmed with Trimmomatric[119] v0.36, with the following parameters differing from default settings: LEADING:0 TRAILING:0 SLIDINGWINDOW:4:15 MINLEN:25. The reference genome was indexed with bowtie2-build with default settings. Paired reads were aligned to the reference genome using bowtie2 with default settings (v2.3.4.1)[120]. In the case of the A-strain, the reference genome was edited to reflect the base substitution within *pyk1*. Aligned reads were counted using *intersect* from the bedtools package (v2.27.1)[121], with the parameters *-wb -f 0.55 -s -bed*. Identical reads were only counted once.
Readcounts were tested for differential expression between strains using DESeq2 v1.18.1, with default settings[122].

Proteomics experiments

Sample preparation for mass spectrometry: Cells were washed with 1X PBS and centrifuged for 3 min at 600 x g at room temperature. Subsequently, cells were washed with 1 ml room temperature lysis buffer (LB: 100 mM HEPES, 1 mM $MgCl_2$, 150 mM KCl, pH 7.5), transferred to 1.5 ml tubes and centrifuged at 600 x g for 5 min at room temperature. After discarding the supernatant, the cell pellets were flash-frozen at -80°C and stored until use. To lyse the cells, pellets were resuspended in 400 µl cold LB and mixed with the same volume of acid-washed glass beads (Sigma Aldrich). The mixture was then transferred to a FastPrep-24TM 5G Instrument (MP Biomedicals) where the cells were disrupted at 4°C by 8 rounds of beads-beating at 30 sec with 200 sec pause between the runs. Samples were then centrifuged at 1000 x g for 2 min at 4°C. The supernatant was collected and protein concentration determined with the bicinchoninic acid assay (Thermo Fisher Scientific). Then, 100 µg of proteome samples were subjected to the sample preparation workflow for MS analysis. In the first step, sodium deoxycholate (Sigma Aldrich) was added to the samples to a final concentration of 5% followed by the addition of Tris(2-carboxyethyl)phosphine (Thermo Fisher Scientific) to a final concentration of 10 mM and incubation at 37°C for 30 min under shaking at 550 rpm to reduce disulfide bridges. Next, the alkylation of free cysteine residues was achieved by adding iodoacetamide (Sigma Aldrich) at 40 mM final concentration. After 45 min incubation at room temperature in the dark, samples were diluted 1:5 with freshly prepared 0.1M ammonium bicarbonate and pre-digested with lysyl endopeptidase LysC (Wako Chemicals) at an enzyme to substrate (E/S) ratio of 1:100 for 4 h at 37°C under shaking at 800 rpm. Digestion was completed by treatment with sequencing-grade trypsin (promega) at an E/S ratio of 1:100 for 16h at 37°C, under shaking at 180 rpm. Protease digestions were quenched by lowering the reaction pH to <3 with the addition of formic acid to a final concentration of 1%. Peptides were desalted using Sep-Pak C18 cartridges according to manufacturer's instructions (Waters). After elution from the cartridges, peptides were dried using a vacuum centrifuge and resuspended in 50 µl 0.1% formic acid for MS measurement. LC-MS/MS data acquisition: Peptide samples were analyzed on an Orbitrap Q Exactive Plus mass spectrometer (Thermo Fisher Scientific) equipped with a nano-electrospray ion source and a nano-flow LC system (Easy-nLC 1000, Thermo Fisher Scientific). Peptides were separated on a 40 cm x 0.75 µm i.d. column (New Objective, PF360-75-10-N-5) packed in house with 1.9 um C18 beads (Dr. Maisch Reprosil-Pur 120). For LC fractionation, buffer A was 0.1% formic acid and buffer B was 0.1% formic

acid in 100% acetonitrile and the following gradient was employed: linear from 5% to 25% buffer B over 100 min, linear from 25% to 40% buffer B over 10 min, linear from 40% to 90 % buffer B over 5 min. and isocratic with buffer B concentration fixed at 90% for 5 min. The flow rate was 300 nL/min and the column was heated to 50 °C. For shotgun LC-MS/MS data acquisition (DDA), 1 µL peptide digests from each sample were injected independently at a concentration of 1 µg/uL. MS1 spectra were acquired from 350 to 1500 m/z at a resolution of 70000. The 20 most intense precursors that exceeded 1300 ion counts were selected for fragmentation at 25 eV normalized collision energy and the corresponding MS2 spectra were acquired at a resolution of 17500 using maximally 100,000 ions, collected for maximally 55 msec. All multiply charged ions were used to trigger MS-MS scans followed by a dynamic exclusion for 30 sec. Singly charged precursor ions and ions of undefinable charged states were excluded from fragmentation. One µL peptide digest from the same samples were also measured in data-independent acquisition (DIA) mode on an Orbitrap QExactive Plus mass spectrometer (Thermo Fisher Scientific) using the DIA settings reported[123].

Peptide identification and spectral library generation: The collected DDA spectra were searched against the *S. pombe* fasta database (PMID:25432776), using the Sorcerer™-SEQUEST® database search engine (Thermo Electron), allowing up to two missed cleavages. Cysteine carboxyamidomethylation (+57.0214 Da) and methionine oxidation (+15.99492) were allowed as fixed and variable modifications, respectively. Monoisotopic peptide tolerance was set to 10 ppm, and fragment mass tolerance was set to 0.02 Da. The identified proteins were filtered using the high peptide confidence setting in Protein Discoverer (version 2.2, Thermo Fisher Scientific), which correspond to a filter for 1% FDR on peptide level. For generation of spectral libraries, the DDA spectra were analyzed with Proteome Discoverer 2.2 as described above and imported in the Spectronaut software (version 8,Biognosys AG)[124]. DIA-MS targeted data extraction was performed with Spectronaut version 8 (Biognosys AG)[124] with default settings. Retention time prediction type was set to dynamic iRT with correction factor 1 for determination of XIC extraction windows. Retention time correction was performed with a non-linear calibration strategy, and interference correction on MS2 level was enabled[125]. The false discovery rate (FDR) was estimated with the mProphet approach[126] and set to 1% at peptide precursor level.

Analysis of protein abundances: Analyses of protein abundance were performed with the MSstat package[127]. Unless stated otherwise, default parameters were used. Spectronaut output was converted to the input format of MSstats with the *SpectronauttoMSstatsFormat* function. The normalised peak areas were further processed with the function *dataProcess* and *intensity* = *"NormalizedPeakArea"*. This included log2 transformation, median normalization, the summary of fragments to peptides, and the summary of peptides to proteins. The parameter *featureSubset* was set to “all”. We used the *groupComparison* function with linear mixed models to compare protein abundances between the replicates for the two strains. The FDRs and log2 fold changes between strains (l2FCs) returned by *groupComparison* were used for further analyses.

Functional enrichment analyses

Gene ontology (GO) enrichment analysis was performed with the *topGO* package (v2.30.1)[128]. The annotations were downloaded from pombase.com (uploaded on 1st Sept 2015)[49]. The transcriptome and proteome were tested separately. All genes with an FDR

≤10% were included in the test set, while all other genes formed the background. Importantly, only those genes with available measurements were included in the background to avoid false positive enrichments. The *nodeSize* was set to 10. We performed Fisher's exact tests with the *elim*-algorithm. All terms with p ≤0.01 were included in the plots. We used AnGeLi[74] for functional enrichment analysis to confirm the GO enrichments and to reveal overlap with core environmental stress and TORC1 response genes.

Metabolomics experiments

Overnight, cell pre-cultures were diluted to OD_{600} of 0.1, and 5 ml were quenched in 20 ml dry-ice-cold methanol when an OD_{600} of 0.8 was reached. This suspension was spun down (600g, 3 min, 4°C) and the supernatant was discarded by inversion. The pellet was resuspended in the remaining liquid and transferred to a small tube, and spun down again with the same parameters. The supernatant was removed completely and the pellet was frozen in liquid nitrogen and stored at -80°C until further processing.

The samples were extracted as described[129]. Acid washed Zirkonia beads were added to the pellet, together with 140 µl of 10:4 MeOH/water, and cells were lysed mechanically (FastPrep Instrument, 40 sec, 6.5 m/s). Then, 50 µl chloroform were added and mixed thoroughly, followed by 50 µl water and 50 µl chloroform. Insoluble components were removed by centrifugation at 5000g for 10 min. The aqueous phase was recovered and used without further conditioning. One microlitre was injected for LC-MS/MS analysis. The sample was diluted 1:20 for the analysis of free amino acids, except for glutamine which was quantified without dilution.

The compounds were resolved on an Agilent 1290 liquid chromatography system, using a HILIC amide column (Waters BEH Amide, 2.1 x 100 mm, 1.7 µm particle size) with acetonitrile (solvent A) and 100 mM aqueous ammonium carbonate (solvent B) for gradient elution at a constant flow rate of 0.3 ml/min and column temperature of 35°C. The gradient program started at 30% B and was kept constant for 3 min before a steady increase to 60% B over 4 min. Solvent B was maintained at 60% for 1 min before returning to initial conditions. The column was washed and equilibrated for 2 min resulting in a total analysis time of 10 min. Compounds were identified by comparing retention time and fragmentation patterns with analytical standards. The samples were analysed by tandem mass spectrometry coupled to an Agilent 6470 triple quadrupole. The sample was acquired using the Agilent dynamic MRM (dMRM) approach with polarity switching. Peak areas were converted to concentrations using external calibration by standard curves and corrected for the optical density of the culture at the time of harvesting.

Enzyme assays

PYK activity was assayed as described[60]. The homothallic A- and T-strains were grown over-night in 3 ml of YES pre-cultures, diluted to OD 0.15 and grown for a further 5 hrs. The OD_{600} of cultures at the time of sampling was approximately 1. Lysate was prepared by spinning 2 ml of culture (800g, 3 min, RT), discarding the supernatant, adding a small amount of glass beads and 200 µL of lysis buffer (10 mM Tris at pH 7, 100 mM KCl, 5 mM MgCl2, 1 mM DTT), breaking the cells with a FastPrep instrument (MP Biomedicals), operated at 4°C three times for 40 sec with 1 min breaks in between, spinning at 8000g (3 min, 4°C), and finally transferring the supernatant to a fresh tube kept on ice and used fresh.

Reactions with a total volume of 200 µl in a 96 well plate contained 10 mM Tris at pH 7, 100 mM KCl, 5 mM $MgCl_2$, 20 µg L-lactate dehydrogenase from rabbit muscle, 5 mM ADP (all by Sigma-Aldrich), 10 mM PEP (from Molekula) and 200µM NADH (from Bioworld). The reaction mix was warmed to 32°C for 1 min and the reaction was started by adding 4 µl of lysate. The absorbance at 340nm was measured every ~15 sec in a Tecan Infinite M200 Pro plate reader set to 32°C. Absorbance values below 0.2 were set to NA. Absorbance values were converted to concentration using the extinction coefficient 6220 M^{-1} cm^{-1} and a path length of 0.5411cm (calculated from reaction volume and well diameter). The slope of the concentration trace was determined using the linregress function from the scipy python package, background subtracted (reaction mix without lysate), and divided by the OD of the culture at the time of sampling.

Oxygen consumption rate measurements

YES cell cultures (100ml) were grown overnight to an OD between 1 and 3. A ~25ml sample was put into a 25ml Erlenmeyer flask and stirred at 900rpm using a magnetic stirrer bar. An oxygen probe (Hanna HI 98193), held with a clamp, was inserted into the flask, resulting in it being completely filled, and the flask was sealed with multiple layers of parafilm. The oxygen saturation of the culture was followed over 7 min and recorded every ~1 min. The slope of the concentration trace was determined using the linregress function from the scipy python package and divided by the OD of the culture.

Measurement of growth rates

Growth curves shown in Fig. 4A were obtained by pre-culturing cells overnight (5 ml), diluting 1 to 50, growing for an additional 6 hours, and then diluting to OD_{600} 0.2. Growth curves were recorded with a BioLector instrument (m2p-labs). Strains grew in 48 flower-shaped well plates, shaken at 1000 rpm at 85% humidity. Biomass measurements use light scattering at 620 nm and were taken every 10 min, with the signal gain set to 50. The maximum slope was extracted by fitting all possible linear regressions over 12 consecutive timepoints and retaining the one with the highest slope.

Carbon source screen

We used Edinburgh minimal medium (EMM) or YES, depending on the nitrogen source in the final assay medium[130]. Cells were pre-cultured overnight (5 ml), diluted to approximately OD_{600} 0.2 in the morning, grown for 6 hours, spun down (400g, 4 min, RT), washed once in EMM without glucose or YE, resuspended and diluted to OD_{600} 0.2 in EMM without glucose or YE. Carbon sources were used at the same molarity as glucose in standard EMM (2% w/w, 111 mM), except for sucrose, maltose and raffinose (where amount was corrected for number of monosaccharides they contain), pectin (where a saturated solution was used), and glutamine (16% w/w due to low solubility). The OD_{600} was recorded in 384-well plates, every 15 min, with short shaking (15 sec) before each measurement in a plate reader (Tecan Infinite M200 Pro). Growth curves were smoothed by first applying a median filter of size 5 and a Gaussian filter with sigma=3. We obtained maximum slopes for each well by fitting all linear regression models for 12 timepoints over the course of the growth curve and retaining the best one.

Biolog phenotyping screen

The resistance to various chemical compounds was assessed using Biolog Phenotype MicroArray plates PM22, PM23 and PM25. JB50 and *pyk1*-A-allele h^{90} were grown overnight in EMM, diluted to OD_{600} 0.15 in fresh EMM, and grown for 6 hours at 25°C. Cultures were then diluted to OD_{600} 0.05 and 100 µl were added to each well. For each plate type, two individual plates were used (one per strain). Growth curves were recorded by measuring the absorbance at 610 nm every 30 min in an EnVision 2104 plate reader (PerkinElmer) with stacker module. The room was not strictly temperature controlled but was stable at 23.5±1°C over the course of the experiment. Growth curves exhibited considerable noise levels and were smoothed by first applying a median filter of size 5 and a Gaussian filter with sigma=3. We obtained maximum slopes for each well by fitting all linear regression models for 12 timepoints over the course of the growth curve and retaining the best one. Each plate contained multiple concentrations of the same compound, and dose-response curves were plotted for all (Supplement), with hits identified by manual inspection.

To assess the ability of both strains for using different nitrogen sources (Biolog Phenotype MicroArray plate PM3), we applied the same strategy with the following modifications. We used strains with the heterothallic h^- mating type to prevent mating and sporulation in poor nutrient conditions. Pre-cultures were diluted to OD_{600} 0.2 and grown for 6 hours at 25°C. Cultures were then spun down (300g, 3 min, RT), washed in EMM without nitrogen or carbon (EMM-N-C), resuspended in EMM-N at an OD_{600} of 0.2 and 100 µl of cells were added to each well of the assay plates. OD_{610} was recorded in 15 min intervals, and the fit range for maximum slope extraction was accordingly doubled to 24 timepoints. Growth curves were otherwise acquired and analysed similarly. Nitrogen sources in which both strains had a maximum growth rate <0.015 were excluded from further analysis.

Spot assays

Three independent pre-cultures were used for the T-strain and one pre-culture per independent CRISPR-engineered mutant. Pre-cultures were grown in either YES or EMM media depending on the plate used for the actual assay. Overnight cultures were diluted to OD_{600} of 0.15 and grown for an additional ~6 hours. Cultures were then diluted to OD_{600} of 0.4, with a 3-fold dilution series prepared in a 96-well plate (one culture per column). The '1 to 16 array single source' program of the RoToR HDA (Singer Instruments) was used to create the readout plates. For each batch, a control plate without toxin was prepared to check for any accidental bias in strain dilutions.

Chronological lifespan assay

Chronological lifespan assays were performed as previously described[58]. Single colonies were picked and inoculated in YES. Cells were grown for 48 hours, which was treated as the beginning of stationary phase (Day 0). Error bars in Fig. 4G represent the standard deviation of 3 independent biological repeats, which consist of 3 technical repeats each, averaged previously. For the A-strain, 3 different mutants were used as biological repeats.

Supplementary information and availability of materials

The homothallic and heterothallic A-strains (*972 h-* pyk1^{T343A} and *968 h90* pyk1^{T343A} respectively) are available from the Bähler Laboratory on request.

Supplementary Data includes:

Supplementary Table 1: GWAS phenotypes
Supplementary Table 2: GWAS top hits
Supplementary Table 3: Metabolomics data set
Supplementary Table 4: Gene expression data set
Supplementary Table 5: GO-enrichments of genes regulated only on the protein level
Supplementary Table 6: GO-enrichments of genes regulated on both the transcript and protein level
Supplementary Table 7: Carbon Source screen
Supplementary Table 8: Nitrogen Source screen

Supplementary Figure 1: Fitness on YES and YES+antimycin
Supplementary Figure 2: Metabolome Boxplots
Supplementary Figure 3: Additional transcriptome analysis
Supplementary Figure 4: Additional proteome analysis
Supplementary Figure 5: Differential abundance of transcripts and proteins
Supplementary Figure 6: Biolog Drug Screen Dose Response Curves

Supplementary figures
https://drive.google.com/file/d/1iD0beZCqSBfzTlzM5ucb4EYeOS6l59Zk/view?usp=sharing

And supplementary tables here:
https://drive.google.com/file/d/1UkLITBnhJsS42pYc62vsqHNeGPkzwimF/view?usp=sharing

Acknowledgements

We are grateful to the Francis Crick Institute Bioinformatics Core facility for advice on phylogenetic trees, Doug Speed for advice on heritability estimation and GWAS, Jamie Macpherson for advice on PYK activity assays, and David Ellis for critical reading of the manuscript. JG received funding from the DFG (Grants CRC 680 and CRC 1310). ST was supported by a Boehringer Ingelheim Fonds PhD Fellowship. This work was supported by a Wellcome Trust Senior Investigator Award (095598/Z/11/Z) to JB. The Francis Crick Institute receives its core funding from Cancer Research UK (FC001134), the UK Medical Research Council (FC001134), and the Wellcome Trust (FC001134).

References

1. New, A. M. *et al*. Different levels of catabolite repression optimize growth in stable and variable environments. *PLoS Biol*. **12**, e1001764 (2014).
2. Valvezan, A. J. & Manning, B. D. Molecular logic of mTORC1 signalling as a metabolic rheostat. *Nature Metabolism* **1**, 321–333 (2019).
3. Wallace, D. C. & Fan, W. Energetics, epigenetics, mitochondrial genetics. *Mitochondrion* **10**, 12–31 (2010).
4. Zanella, A., Fermo, E., Bianchi, P. & Valentini, G. Red cell pyruvate kinase deficiency: molecular and clinical aspects. *Br. J. Haematol*. **130**, 11–25 (2005).
5. Djouadi, F. & Bastin, J. Mitochondrial Genetic Disorders: Cell Signaling and Pharmacological Therapies. *Cells* **8**, (2019).
6. Molenaar, D., van Berlo, R., de Ridder, D. & Teusink, B. Shifts in growth strategies reflect tradeoffs in cellular economics. *Mol. Syst. Biol*. **5**, 323 (2009).
7. Takeda, K., Starzynski, C., Mori, A. & Yanagida, M. The critical glucose concentration for respiration-independent proliferation of fission yeast, Schizosaccharomyces pombe. *Mitochondrion* **22**, 91–95 (2015).
8. Crabtree, H. G. Observations on the carbohydrate metabolism of tumours. *Biochem. J* **23**, 536–545 (1929).
9. Pfeiffer, T. & Morley, A. An evolutionary perspective on the Crabtree effect. *Front Mol Biosci* **1**, 17 (2014).
10. Warburg, O. The metabolism of tumors in the body. *The Journal of General Physiology* **8**, 519–530 (1927).
11. Diaz-Ruiz, R., Uribe-Carvajal, S., Devin, A. & Rigoulet, M. Tumor cell energy metabolism and its common features with yeast metabolism. *Biochim. Biophys. Acta* **1796**, 252–265 (2009).
12. Lunt, S. Y. & Vander Heiden, M. G. Aerobic Glycolysis: Meeting the Metabolic Requirements of Cell Proliferation. *Annual Review of Cell and Developmental Biology* **27**, 441–464 (2011).
13. Costa, A. S. H. & Frezza, C. Metabolic Reprogramming and Oncogenesis. *International Review of Cell and Molecular Biology* 213–231 (2017). doi:10.1016/bs.ircmb.2017.01.001
14. Basan, M. *et al*. Overflow metabolism in Escherichia coli results from efficient proteome allocation. *Nature* **528**, 99–104 (2015).
15. Mori, M., Marinari, E. & De Martino, A. A yield-cost tradeoff governs Escherichia coli's decision between fermentation and respiration in carbon-limited growth. *Systems Biology and Applications* **5**, (2019).
16. Andersen, K. B. & von Meyenburg, K. Are growth rates of Escherichia coli in batch cultures limited by respiration? *J. Bacteriol*. **144**, 114–123 (1980).
17. Zhuang, K., Vemuri, G. N. & Mahadevan, R. Economics of membrane occupancy and respiro-fermentation. *Mol. Syst. Biol*. **7**, 500 (2011).
18. Vazquez, A. & Oltvai, Z. N. Macromolecular crowding explains overflow metabolism in cells. *Sci. Rep*. **6**, 31007 (2016).
19. Szenk, M., Dill, K. A. & de Graff, A. M. R. Why Do Fast-Growing Bacteria Enter Overflow Metabolism? Testing the Membrane Real Estate Hypothesis. *Cell Syst* **5**, 95–104 (2017).
20. Dai, Z., Shestov, A. A., Lai, L. & Locasale, J. W. A Flux Balance of Glucose Metabolism Clarifies the Requirements of the Warburg Effect. *Biophys. J*. **111**, 1088–1100 (2016).
21. Alteriis, E. de *et al*. Revisiting the Crabtree/Warburg effect in a dynamic perspective: a fitness advantage against sugar-induced cell death. *Cell Cycle* **17**, 688–701 (2018).
22. Groot, D. H. de *et al*. The number of active metabolic pathways is bounded by the number of cellular constraints at maximal metabolic rates. *PLOS Computational Biology* **15**, e1006858 (2019).
23. Skinner, C. & Lin, S.-J. Effects of calorie restriction on life span of microorganisms. *Appl. Microbiol. Biotechnol*. **88**, 817–828 (2010).
24. Chan, K. & Roth, M. B. Anoxia-induced suspended animation in budding yeast as an experimental paradigm for studying oxygen-regulated gene expression. *Eukaryot. Cell* **7**, 1795–1808 (2008).
25. Ephrussi, B., Hottinguer, H., Tavlitzki, J. Action de l'acriflavine sur les levures. I. La mutation 'petite colonie.' *Ann. Inst. Pasteur* **76**, 351–367 (1949).
26. Haffter, P. & Fox, T. D. Nuclear mutations in the petite-negative yeast Schizosaccharomyces pombe allow growth of cells lacking mitochondrial DNA. - PubMed - NCBI. Available at: https://www.ncbi.nlm.nih.gov/pubmed/1644270. (Accessed: 24th January 2019)
27. Heslot, H., Goffeau, A. & Louis, C. Respiratory Metabolism of a 'Petite Negative' Yeast Schizosaccharomyces pombe 972h−. *J. Bacteriol*. **104**, 473–481 (1970).
28. Chiron, S. *et al*. Studying Mitochondria in an Attractive Model: Schizosaccharomyces pombe. *Methods in Molecular Biology* 91–105 (2007). doi:10.1007/978-1-59745-365-3_7
29. Malecki, M. *et al*. Functional and regulatory profiling of energy metabolism in fission yeast. *Genome Biol*.

17, 240 (2016).
30. Zuin, A. *et al*. Lifespan extension by calorie restriction relies on the Sty1 MAP kinase stress pathway. *EMBO J.* **29**, 981–991 (2010).
31. DeRisi, J. L., Iyer, V. R. & Brown, P. O. Exploring the metabolic and genetic control of gene expression on a genomic scale. *Science* **278**, 680–686 (1997).
32. Jeffares, D. C. *et al*. The genomic and phenotypic diversity of Schizosaccharomyces pombe. *Nat. Genet.* **47**, 235–241 (2015).
33. Yu, T. *et al*. Reprogramming Yeast Metabolism from Alcoholic Fermentation to Lipogenesis. *Cell* **174**, 1549–1558.e14 (2018).
34. Grüning, N.-M. *et al*. Pyruvate Kinase Triggers a Metabolic Feedback Loop that Controls Redox Metabolism in Respiring Cells. *Cell Metab.* **14**, 415–427 (2011).
35. Pearce, A. K. *et al*. Pyruvate kinase (Pyk1) levels influence both the rate and direction of carbon flux in yeast under fermentative conditions. *Microbiology* **147**, 391–401 (2001).
36. Muñoz, M. E. & Ponce, E. Pyruvate kinase: current status of regulatory and functional properties. *Comp. Biochem. Physiol. B Biochem. Mol. Biol.* **135**, 197–218 (2003).
37. Allert, S., Ernest, I., Poliszczak, A., Opperdoes, F. R. & Michels, P. A. Molecular cloning and analysis of two tandemly linked genes for pyruvate kinase of Trypanosoma brucei. *Eur. J. Biochem.* **200**, 19–27 (1991).
38. Israelsen, W. J. & Vander Heiden, M. G. Pyruvate kinase: Function, regulation and role in cancer. *Semin. Cell Dev. Biol.* **43**, 43–51 (2015).
39. Bradley, P. H., Gibney, P. A., Botstein, D., Troyanskaya, O. G. & Rabinowitz, J. D. Minor Isozymes Tailor Yeast Metabolism to Carbon Availability. *mSystems* **4**, (2019).
40. Bluemlein, K. *et al*. No evidence for a shift in pyruvate kinase PKM1 to PKM2 expression during tumorigenesis. *Oncotarget* **2**, 393–400 (2011).
41. Nairn, J. *et al*. Cloning and sequencing of a gene encoding pyruvate kinase from Schizosaccharomyces pombe; implications for quaternary structure and regulation of the enzyme. *FEMS Microbiol. Lett.* **134**, 221–226 (1995).
42. Kim, H. *et al*. Structure of Antimycin A1, a Specific Electron Transfer Inhibitor of Ubiquinol−CytochromecOxidoreductase. *J. Am. Chem. Soc.* **121**, 4902–4903 (1999).
43. Malecki, M. & Bähler, J. Identifying genes required for respiratory growth of fission yeast. *Wellcome Open Res* **1**, 12 (2016).
44. Rhind, N. *et al*. Comparative functional genomics of the fission yeasts. *Science* **332**, 930–936 (2011).
45. Katoh, K., Rozewicki, J. & Yamada, K. D. MAFFT online service: multiple sequence alignment, interactive sequence choice and visualization. *Brief. Bioinform.* (2017). doi:10.1093/bib/bbx108
46. Waterhouse, A. M., Procter, J. B., Martin, D. M. A., Clamp, M. & Barton, G. J. Jalview Version 2--a multiple sequence alignment editor and analysis workbench. *Bioinformatics* **25**, 1189–1191 (2009).
47. Peter, J. *et al*. Genome evolution across 1,011 Saccharomyces cerevisiae isolates. *Nature* **556**, 339–344 (2018).
48. Cingolani, P. *et al*. A program for annotating and predicting the effects of single nucleotide polymorphisms, SnpEff: SNPs in the genome of Drosophila melanogaster strain w1118; iso-2; iso-3. *Fly* **6**, 80–92 (2012).
49. Wood, V. *et al*. PomBase: a comprehensive online resource for fission yeast. *Nucleic Acids Res.* **40**, D695–9 (2012).
50. Hu, W. *et al*. A large gene family in fission yeast encodes spore killers that subvert Mendel's law. *Elife* **6**, (2017).
51. Boles, E. *et al*. Characterization of a glucose-repressed pyruvate kinase (Pyk2p) in Saccharomyces cerevisiae that is catalytically insensitive to fructose-1,6-bisphosphate. *J. Bacteriol.* **179**, 2987–2993 (1997).
52. Wood, V. *et al*. The genome sequence of Schizosaccharomyces pombe. *Nature* **415**, 871–880 (2002).
53. Camacho, C. *et al*. BLAST+: architecture and applications. *BMC Bioinformatics* **10**, 421 (2009).
54. Rodríguez-López, M. *et al*. A CRISPR/Cas9-based method and primer design tool for seamless genome editing in fission yeast. *Wellcome Open Res* **1**, 19 (2016).
55. Nairn, J. *et al*. Purification and characterization of pyruvate kinase from Schizosaccharomyces pombe: evidence for an unusual quaternary structure. *Protein Expr. Purif.* **14**, 247–253 (1998).
56. Gruning, N. M. N.-M. *et al*. Inhibition of triosephosphate isomerase by phosphoenolpyruvate in the feedback-regulation of glycolysis. *Open Biol.* **4**, 130232–130232 (2014).
57. Bluemlein, K. *et al*. Pyruvate kinase is a dosage-dependent regulator of cellular amino acid homeostasis. *Oncotarget* **2**, 393–400 (2012).
58. Rallis, C., Codlin, S. & Bähler, J. TORC1 signaling inhibition by rapamycin and caffeine affect lifespan, global gene expression, and cell proliferation of fission yeast. *Aging Cell* **12**, 563–573 (2013).

59. Chen, D. *et al*. Global transcriptional responses of fission yeast to environmental stress. *Mol. Biol. Cell* **14**, 214–229 (2003).
60. Gehrig, S. *et al*. An engineered photoswitchable mammalian pyruvate kinase. *FEBS J.* **284**, 2955–2980 (2017).
61. Litsios, A., Ortega, Á. D., Wit, E. C. & Heinemann, M. Metabolic-flux dependent regulation of microbial physiology. *Curr. Opin. Microbiol.* **42**, 71–78 (2018).
62. Christen, S. & Sauer, U. Intracellular characterization of aerobic glucose metabolism in seven yeast species by 13C flux analysis and metabolomics. *FEMS Yeast Res.* **11**, 263–272 (2011).
63. Huberts, D. H. E. W., Niebel, B. & Heinemann, M. A flux-sensing mechanism could regulate the switch between respiration and fermentation. *FEMS Yeast Res.* **12**, 118–128 (2012).
64. Atkinson, D. E. & Walton, G. M. Adenosine triphosphate conservation in metabolic regulation. Rat liver citrate cleavage enzyme. *J. Biol. Chem.* **242**, 3239–3241 (1967).
65. De la Fuente, I. M. *et al*. On the dynamics of the adenylate energy system: homeorhesis vs homeostasis. *PLoS One* **9**, e108676 (2014).
66. Blacker, T. S. & Duchen, M. R. Investigating mitochondrial redox state using NADH and NADPH autofluorescence. *Free Radic. Biol. Med.* **100**, 53–65 (2016).
67. Vivancos, A. P., Jara, M., Zuin, A., Sansó, M. & Hidalgo, E. Oxidative stress in Schizosaccharomyces pombe: different H2O2 levels, different response pathways. *Mol. Genet. Genomics* **276**, 495–502 (2006).
68. Drakulic, T. *et al*. Involvement of oxidative stress response genes in redox homeostasis, the level of reactive oxygen species, and ageing in Saccharomyces cerevisiae. *FEMS Yeast Res.* **5**, 1215–1228 (2005).
69. Veal, E. A., Tomalin, L. E., Morgan, B. A. & Day, A. M. The fission yeast Schizosaccharomyces pombe as a model to understand how peroxiredoxins influence cell responses to hydrogen peroxide. *Biochem. Soc. Trans.* **42**, 909–916 (2014).
70. Carmel-Harel, O. & Storz, G. Roles of the glutathione- and thioredoxin-dependent reduction systems in the Escherichia coli and saccharomyces cerevisiae responses to oxidative stress. *Annu. Rev. Microbiol.* **54**, 439–461 (2000).
71. Sun, F., Dai, C., Xie, J. & Hu, X. Biochemical issues in estimation of cytosolic free NAD/NADH ratio. *PLoS One* **7**, e34525 (2012).
72. Lu, W., Wang, L., Chen, L., Hui, S. & Rabinowitz, J. D. Extraction and Quantitation of Nicotinamide Adenine Dinucleotide Redox Cofactors. *Antioxid. Redox Signal.* **28**, 167–179 (2018).
73. Viljoen, M., Subden, R. E., Krizus, A. & Van Vuuren, H. J. Molecular analysis of the malic enzyme gene (mae2) of Schizosaccharomyces pombe. *Yeast* **10**, 613–624 (1994).
74. Bitton, D. A. *et al*. AnGeLi: A Tool for the Analysis of Gene Lists from Fission Yeast. *Frontiers in Genetics* **6**, (2015).
75. Ferenci, T. Trade-off Mechanisms Shaping the Diversity of Bacteria. *Trends Microbiol.* **24**, 209–223 (2016).
76. Zakrzewska, A. *et al*. Genome-wide analysis of yeast stress survival and tolerance acquisition to analyze the central trade-off between growth rate and cellular robustness. *Mol. Biol. Cell* **22**, 4435–4446 (2011).
77. López-Maury, L., Marguerat, S. & Bähler, J. Tuning gene expression to changing environments: from rapid responses to evolutionary adaptation. *Nat. Rev. Genet.* **9**, 583–593 (2008).
78. Anastasiou, D. *et al*. Inhibition of pyruvate kinase M2 by reactive oxygen species contributes to cellular antioxidant responses. *Science* **334**, 1278–1283 (2011).
79. Ito, A. *et al*. The screening of hydrogen peroxide-producing lactic acid bacteria and their application to inactivating psychrotrophic food-borne pathogens. *Curr. Microbiol.* **47**, 231–236 (2003).
80. Ponomarova, O. *et al*. Yeast Creates a Niche for Symbiotic Lactic Acid Bacteria through Nitrogen Overflow. *Cell Syst* **5**, 345–357.e6 (2017).
81. De Filippi, L. *et al*. Membrane stress is coupled to a rapid translational control of gene expression in chlorpromazine-treated cells. *Curr. Genet.* **52**, 171–185 (2007).
82. Lin, Y. *et al*. The antituberculosis antibiotic capreomycin inhibits protein synthesis by disrupting interaction between ribosomal proteins L12 and L10. *Antimicrob. Agents Chemother.* **58**, 2038–2044 (2014).
83. Oustrin, M. L., Belenguer, P., Leroy, D., Hoffmann, I. & Ducommun, B. Effect of phenylarsine oxide on the fission yeast Schizosaccharomyces pombe cell cycle. *Biochimie* **77**, 279–287 (1995).
84. Reuben, J. & Kayne, F. J. Thallium-205 nuclear magnetic resonance study of pyruvate kinase and its substrates. Evidence for a substrate-induced conformational change. *J. Biol. Chem.* **246**, 6227–6234 (1971).
85. Kayne, F. J. Thallium (I) activation of pyruvate kinase. *Arch. Biochem. Biophys.* **143**, 232–239 (1971).
86. Rhodes, N., Morris, C. N., Ainsworth, S. & Kinderlerer, J. The regulatory properties of yeast pyruvate kinase. Effects of NH4+ and K+ concentrations. *Biochem. J* **234**, 705–715 (1986).
87. Al-Regaiey, K. A. The effects of calorie restriction on aging: a brief review. *Eur. Rev. Med. Pharmacol.*

Sci. **20**, 2468–2473 (2016).
88. Bonawitz, N. D., Chatenay-Lapointe, M., Pan, Y. & Shadel, G. S. Reduced TOR signaling extends chronological life span via increased respiration and upregulation of mitochondrial gene expression. *Cell Metab*. **5**, 265–277 (2007).
89. Pan, Y., Schroeder, E. A., Ocampo, A., Barrientos, A. & Shadel, G. S. Regulation of yeast chronological life span by TORC1 via adaptive mitochondrial ROS signaling. *Cell Metab*. **13**, 668–678 (2011).
90. Roux, A. E. *et al*. Pro-aging effects of glucose signaling through a G protein-coupled glucose receptor in fission yeast. *PLoS Genet*. **5**, e1000408 (2009).
91. Smith, J. T., White, J. W., Dungrawala, H., Hua, H. & Schneider, B. L. Yeast lifespan variation correlates with cell growth and SIR2 expression. *PLoS One* **13**, e0200275 (2018).
92. Janssens, G. E. & Veenhoff, L. M. The Natural Variation in Lifespans of Single Yeast Cells Is Related to Variation in Cell Size, Ribosomal Protein, and Division Time. *PLoS One* **11**, e0167394 (2016).
93. Yang, J. *et al*. Cell size and growth rate are major determinants of replicative lifespan. *Cell Cycle* **10**, 144–155 (2011).
94. Rallis, C., López-Maury, L., Georgescu, T., Pancaldi, V. & Bähler, J. Systematic screen for mutants resistant to TORC1 inhibition in fission yeast reveals genes involved in cellular ageing and growth. *Biol. Open* **3**, 161–171 (2014).
95. Ralser, M. *et al*. Dynamic rerouting of the carbohydrate flux is key to counteracting oxidative stress. *J. Biol*. **6**, 10 (2007).
96. Slavov, N. & Botstein, D. Decoupling nutrient signaling from growth rate causes aerobic glycolysis and deregulation of cell size and gene expression. *Mol. Biol. Cell* **24**, 157–168 (2013).
97. Hesketh, A., Vergnano, M. & Oliver, S. G. Determination of the Global Pattern of Gene Expression in Yeast Cells by Intracellular Levels of Guanine Nucleotides. *MBio* **10**, (2019).
98. Pir, P. *et al*. The genetic control of growth rate: a systems biology study in yeast. *BMC Syst. Biol*. **6**, 4 (2012).
99. Tamari, Z., Rosin, D., Voichek, Y. & Barkai, N. Coordination of gene expression and growth-rate in natural populations of budding yeast. *PLoS One* **9**, e88801 (2014).
100. Morano, K. A., Grant, C. M. & Moye-Rowley, W. S. The response to heat shock and oxidative stress in Saccharomyces cerevisiae. *Genetics* **190**, 1157–1195 (2012).
101. Christofk, H. R. *et al*. The M2 splice isoform of pyruvate kinase is important for cancer metabolism and tumour growth. *Nature* **452**, 230–233 (2008).
102. Allen, A. E. & Locasale, J. W. Glucose Metabolism in Cancer: The Saga of Pyruvate Kinase Continues. *Cancer Cell* **33**, 337–339 (2018).
103. Lunt, S. Y. *et al*. Pyruvate Kinase Isoform Expression Alters Nucleotide Synthesis to Impact Cell Proliferation. *Molecular Cell* **57**, 95–107 (2015).
104. Morita, M. *et al*. PKM1 Confers Metabolic Advantages and Promotes Cell-Autonomous Tumor Cell Growth. *Cancer Cell* **33**, 355–367.e7 (2018).
105. Wagih, O. & Parts, L. gitter: a robust and accurate method for quantification of colony sizes from plate images. *G3* **4**, 547–552 (2014).
106. Zackrisson, M. *et al*. Scan-o-matic: High-Resolution Microbial Phenomics at a Massive Scale. *G3* **6**, 3003–3014 (2016).
107. Pedregosa, F. *et al*. Scikit-learn: Machine Learning in Python. *J. Mach. Learn. Res*. **12**, 2825–2830 (2011).
108. Garrison, E. & Marth, G. Haplotype-based variant detection from short-read sequencing. *arXiv [q-bio.GN]* (2012).
109. Li, H. *et al*. The Sequence Alignment/Map format and SAMtools. *Bioinformatics* **25**, 2078–2079 (2009).
110. Danecek, P. *et al*. The variant call format and VCFtools. *Bioinformatics* **27**, 2156–2158 (2011).
111. Purcell, S. *et al*. PLINK: A Tool Set for Whole-Genome Association and Population-Based Linkage Analyses. *Am. J. Hum. Genet*. **81**, 559–575 (2007).
112. Speed, D., Hemani, G., Johnson, M. R. & Balding, D. J. Improved heritability estimation from genome-wide SNPs. *Am. J. Hum. Genet*. **91**, 1011–1021 (2012).
113. Speed, D. *et al*. Reevaluation of SNP heritability in complex human traits. *Nat. Genet*. **49**, 986–992 (2017).
114. Cook, D. E. & Andersen, E. C. VCF-kit: assorted utilities for the variant call format. *Bioinformatics* **33**, 1581–1582 (2017).
115. Larkin, M. A. *et al*. Clustal W and Clustal X version 2.0. *Bioinformatics* **23**, 2947–2948 (2007).
116. Goujon, M. *et al*. A new bioinformatics analysis tools framework at EMBL-EBI. *Nucleic Acids Res*. **38**, W695–9 (2010).
117. Gouy, M., Guindon, S. & Gascuel, O. SeaView version 4: A multiplatform graphical user interface for sequence alignment and phylogenetic tree building. *Mol. Biol. Evol*. **27**, 221–224 (2010).
118. Lyne, R. *et al*. Whole-genome microarrays of fission yeast: characteristics, accuracy, reproducibility, and

processing of array data. *BMC Genomics* **4**, 27 (2003).
119. Bolger, A. M., Lohse, M. & Usadel, B. Trimmomatic: a flexible trimmer for Illumina sequence data. *Bioinformatics* **30**, 2114–2120 (2014).
120. Langmead, B. & Salzberg, S. L. Fast gapped-read alignment with Bowtie 2. *Nat. Methods* **9**, 357–359 (2012).
121. Quinlan, A. R. & Hall, I. M. BEDTools: a flexible suite of utilities for comparing genomic features. *Bioinformatics* **26**, 841–842 (2010).
122. Love, M. I., Huber, W. & Anders, S. Moderated estimation of fold change and dispersion for RNA-seq data with DESeq2. *Genome Biol.* **15**, 550 (2014).
123. Piazza, I. *et al.* A Map of Protein-Metabolite Interactions Reveals Principles of Chemical Communication. *Cell* **172**, 358–372.e23 (2018).
124. Bruderer, R. *et al.* Extending the limits of quantitative proteome profiling with data-independent acquisition and application to acetaminophen-treated three-dimensional liver microtissues. *Mol. Cell. Proteomics* **14**, 1400–1410 (2015).
125. Bilbao, A. *et al.* Processing strategies and software solutions for data-independent acquisition in mass spectrometry. *Proteomics* **15**, 964–980 (2015).
126. Reiter, L. *et al.* mProphet: automated data processing and statistical validation for large-scale SRM experiments. *Nat. Methods* **8**, 430–435 (2011).
127. Choi, M. *et al.* MSstats: an R package for statistical analysis of quantitative mass spectrometry-based proteomic experiments. *Bioinformatics* **30**, 2524–2526 (2014).
128. Alexa, A., Rahnenführer, J. & Lengauer, T. Improved scoring of functional groups from gene expression data by decorrelating GO graph structure. *Bioinformatics* **22**, 1600–1607 (2006).
129. Bligh, E. G. & Dyer, W. J. A rapid method of total lipid extraction and purification. *Can. J. Biochem. Physiol.* **37**, 911–917 (1959).
130. Moreno, S., Klar, A. & Nurse, P. [56] Molecular genetic analysis of fission yeast Schizosaccharomyces pombe. *Guide to Yeast Genetics and Molecular Biology* 795–823 (1991). doi:10.1016/0076-6879(91)94059-l